Droplet-Level Thermo-mechanical Analysis of the Microcasting Process

R.K. Chin, J.L. Beuth, and C.H. Amon

EDRC 24-120-95

Droplet-Level Thermo-mechanical Analysis of the Microcasting Process

R.K. Chin, J.L. Beuth, and C.H. Amon
Mechanical Engineering Department and the
Engineering Design Research Center
Carnegie Mellon University

This work has been supported by the Engineering Design Research Center, an Engineering Research Center of the National Science Foundation, under Grant No. EEC-8943164, and by the Office of Naval Research under Grant No. N00014-94-1-0183.

Droplet-Level Thermo-mechanical Analysis of the Microcasting Process

R.K. Chin, J.L. Beuth, and C.H. Amon
Mechanical Engineering Department and the
Engineering Design Research Center
Carnegie Mellon University

Abstract

Thermal and mechanical modeling of the microcasting stage of Shape Deposition Manufacturing is presented. Thermal modeling is needed because during the solidification and subsequent cooling of deposited molten metal, thermal aspects determine important effects such as substrate remelting, microstructure development, and build-up of residual stress. Also, temperature control is needed to protect existing machined features. Mechanical modeling is needed because thermally-induced residual stresses can lead to detrimental effects such as part warping, debonding between deposited layers, and reduced apparent strength or life. In this study, thermo-mechanical models of carbon steel deposited onto an existing carbon steel substrate are described.

Current thermal modeling is centered on reliably predicting localized remelting of previously deposited substrate material by newly deposited molten droplets. Temperatures from a one-dimensional model are compared to those obtained at the axis of an axisymmetric model. In this region, the axisymmetric model predicts temperatures that agree with those from the simpler one-dimensional model for times less than that needed for complete droplet solidification.

Current mechanics modeling is centered on the issue of residual stress build-up. The effects of yielding and creep on the build-up of residual stresses are shown. Results show that thermal cycling from newly applied droplets drastically changes the stress state in the top of the substrate. Originally unstressed regions go through a cycle of yield in compression followed by yield in tension. Residual stresses close to the yield stress are predicted during part manufacture. It is likely that these stresses will be substantially relaxed, however, after a part is completed and then separated from the pallet upon which it is built.

Droplet-Level Thermo-mechanical Analysis of the Microcasting Process

R.K. Chin, J.L. Beuth, and C.H. Amon
Mechanical Engineering Department and the
Engineering Design Research Center
Carnegie Mellon University

1. Introduction

Shape Deposition is a manufacturing process under development at Carnegie Mellon which allows the creation of complex three-dimensional parts by the successive deposition of layers of material. After each layer is deposited, it is machined to the required dimensions before depositing the next layer (Merz *et al.*[9] 1994). Shape Deposition Manufacturing combines solid freeform fabrication with other processing operations, such as multi-axis CNC machining, thermal deposition, and shot peening. The benefits of Shape Deposition Manufacturing include the ability to build parts with complicated geometries, multiple materials, and embedded components. But unlike conventional solid freeform fabrication processes, Shape Deposition Manufacturing can also directly build fully dense, functional metal parts to high dimensional accuracy.

Within Shape Deposition Manufacturing, a process for depositing layers is required. The principal deposition process currently in use is termed microcasting, in which droplets of molten material are deposited onto a much cooler substrate. To understand what happens when a droplet lands on a substrate, it is essential to know droplet and substrate temperature histories, for it is the temperature history that determines small-scale behavior such as how deeply the substrate remelts, what microstructures develop in the droplet and the substrate, how strong a bond forms between the droplet and the substrate, and how the droplet flows while it is liquid. Temperature prediction and control are also intimately connected to manufacturing needs such as protection of existing machined surfaces that may or may not be made of a lower melting alloy than the dripped material, protection of embedded sensors, and control of warping and delamination induced by thermal residual stresses.

Residual stresses arise when the hot droplet cools off while it heats up the material underneath, causing differential thermal strains. Residual stresses can lead to reduced apparent strength or life in manufactured parts. This is of particular concern in parts that must withstand substantial mechanical or thermal applied loads. In addition, residual stresses can lead to a number of undesirable effects that are of concern even for parts without significant loading in their application. These effects include part warping, loss of

edge tolerance, and delamination. Residual stress build-up is inherent in any manufacturing process based on successive molten material deposition. Ultimately, in order to control the undesirable effects of residual stresses through process changes and changes in part designs, it is necessary to understand how such stresses build up during manufacture.

The goal of this work is to model Shape Deposition on a droplet or layer level. The temperature distribution in the molten droplet and the substrate and the stresses that build up in the droplet and substrate due to differential thermal strains are investigated from the moment after the droplet spreads out until the temperature distribution becomes uniform. A one-dimensional thermal model is first presented and verified, and then a comparison between the one-dimensional thermal model and an axisymmetric thermal model is made. A one-dimensional mechanical model undergoing thermal loads is checked by using an assumption of pure elastic behavior. Then the effects of yielding and steady-state creep are presented.

2. Numerical Models

Microcasting differs markedly from traditional solidification processes. The several-millimeter-sized droplets are much smaller than typical ingots and castings and yet are larger than the fine droplets (size on the order of 100 |im) used in plasma sprays. In addition, the high-velocity mist of a plasma spray contrasts sharply with the individual droplets of microcasting free-falling to a substrate surface at a rate of several droplets per second. Prior casting models and spray models dealt with lower superheats than those found in microcasting. Prior spray models do not consider substrate remelting, nor do they track the freezing front. Also, the size of microcasted drops and their cooling rates do not demand consideration of undercooling and recalescence, which are important in rapid solidification models (Schmaltz, 1994).

Models have been developed to predict the temperature distributions of processes related to microcasting, such as plasma spraying. For example, El-Kaddah *et al.* (1984) based a one-dimensional analytical temperature solution of the plasma spray process on the solution profiles for the Stefan problem, and then used a finite difference method to extend the solution to reflect the two-dimensional profile of the spray front. Trapaga *et al* (1992) modeled the heat transfer from the sprayed droplet to the substrate by using a heat transfer coefficient. They do not account for heat diffusion or remelting in the substrate. Gao and Sonin (1993) investigated the deposition of wax droplets; however, their use of a Plexiglass target precludes a study of substrate remelting. In the next section, results from a finite element model are compared to the results of Amon *et al.* (1994a), who developed a

one-dimensional finite difference model of the microcasting process in order to predict the depth of the remelted zone in the substrate.

Residual stress modeling has both a thermal aspect and a mechanical aspect. The solution strategy used here is to solve the thermal problem first and then use the temperature solution as an input to the mechanical model. In the mechanical model, loading comes from differential thermal contractions and differential thermal expansions. Because the thermal effects of deformation are assumed to be negligible compared to the thermal effects of heat conduction, the thermal and mechanical models are not coupled. The ABAQUS finite element package was used in this study because of its capability to model both the thermal and mechanical problems. This thermo-mechanical modeling strategy is similar to the strategy employed by Zabaras, Ruan, and Richmond (1991) to model residual stress during the solidification of a casting. Their model accounts for the variation of thermal and mechanical properties with temperature and includes the computational expense of rearranging the spatial mesh after each time step to place the freezing front on element boundaries. Other researchers who link the stress analysis to a thermal analysis include Thomas, Samarasekera, and Brimacombe (1987), who use a very detailed model of steel ingot solidification which, on top of temperature-dependent properties, accounts for time-temperature dependent phase transformations and the volume and property changes associated with those phase changes. The time scale of their process, however, is much longer than the time needed for a single deposited droplet to cool down.

The one-dimensional stress models in this work share some similarities with existing one-dimensional models of solidifying slabs (Weiner and Boley, 1963) and free plates (Landau *et ai,* 1960), and the numerical solution technique shares similarities with the ingot casting work of Thomas *et al.* (1987) and Zabaras *et al* (1991). The solids in the models start off stress-free. But future models used to study sequential droplet or layer deposition will use solid substrates that contain initial stress distributions calculated from the previous deposition. Also, the one-dimensional free plate models lack the protruding feature of a droplet. Axisymmetric or three-dimensional models will be expected to show high stresses and high stress gradients in the vicinity of the droplet.

This work describes the development and verification of two numerical models that calculate the temperature distribution and residual stresses in microcasted carbon steel droplets and a carbon steel substrate. The geometry and time scales used are typical of those normally found in microcasting. The temperature model uses temperature-dependent thermal properties, and the temperature solution is precise enough to determine the location of the freezing front.

There is a need to improve bonding through remelting while keeping temperatures below manufacturing limits and keeping thermal gradients low to decrease residual stresses, for residual stresses cause loss of dimensional tolerance and encourage interlayer debonding. Temperature prediction will be ultimately be used to find improvements in the microcasting process. The predictive capabilities developed will also be integrated with the design of shape-deposited parts.

3. Thermal Model

To accurately solve the problem of a hot liquid droplet landing on a cooler substrate, then solidifying and cooling, requires the use of temperature-dependent properties. It is also necessary to be able to accurately locate the freezing front in order to study the problem of substrate remelting.

To gain confidence in thermal modeling, an ABAQUS model using one-dimensional first-order elements is compared with an independent finite difference model having the same geometry and mesh. Then an axisymmetric model is used to more realistically model the problem of a droplet landing on a large substrate. Temperatures from the one-dimensional model are compared to temperatures along the central axis of the axisymmetric model to determine under what conditions the simpler one-dimensional model gives results that are close to the axisymmetric model. The potential for large savings in computer resources motivates this comparison. Next, the boundary condition at the bottom of the substrate is changed from fixed-temperature to natural convection to determine how sensitive the temperature solution is to the boundary condition at the bottom of the substrate. In Shape Deposition, the substrate is bolted to a pallet, and the actual condition between the substrate and the pallet is conduction across a small contact resistance. By learning what portions of the temperature solution are not strongly influenced by the choice of the boundary condition at the substrate bottom, we also learn when to neglect the modeling error at the substrate bottom.

3.1. One-Dimensional Thermal Model

To gain confidence in the ability of ABAQUS to use temperature-dependent properties and detect the freezing front, temperatures from an ABAQUS finite element solution were compared to those of an independent finite difference solution developed by Amon *et al* (1994a). The geometry of the problem solved consists of a 1 mm layer deposited on top of a 7 mm substrate (see Figure 1). The typical size of an actual deposited layer (prior to machining) would be 2 to 4 mm, although it is possible to deposit a 1 mm layer by properly adjusting manufacturing parameters. The substrate thickness of 7 mm

represents a remote distance from the droplet-substrate interface for numerical modeling purposes. If the droplet is part of the first deposited layer, then an actual typical substrate is 12.7 mm thick. The mesh for the finite difference model contains 161 nodes while the mesh for the finite element model contains 160 one-dimensional first-order elements. In both cases, the mesh is uniform. The temperature-dependent thermal properties used in the model (from Merz, 1994) and shown in Table 1 are those of a low-carbon steel. As indicated in Figure 1, the base of the substrate is held at a constant temperature of 303 K. While the dominant mode of heat transfer is conduction from the droplet into the substrate (Amon *et al,* 1994b), loss of heat from the top of the droplet by natural convection and gain of heat by radiation from the plasma arc are also modeled. Initially, the droplet (the top 1 mm) has a temperature of 2573 K and the substrate (the bottom 7 mm) has a temperature of 303 K. In the finite difference solution, the material is modeled as a pure material with a melting point at 1773 K while in the finite element solution, the material is modeled with a liquidus temperature of 1775 K and a solidus temperature of 1771 K. In both cases, the latent heat of fusion is 270,000 J/kg. In the finite difference solution, the latent heat released at the freezing front causes a discontinuous heat flux at the front:

$$k_s \frac{\partial T}{\partial n}_s - k_l \frac{\partial T}{\partial n}_l = \rho L \frac{\partial s}{\partial t}$$

where

kg = conductivity of the solid at the freezing front

kj = conductivity of the liquid at the freezing front

$\frac{dT}{dn}$ = magnitude of the temperature gradient at the freezing front evaluated on the appropriate side of the front

p = mass density

L = latent heat

$\frac{\partial s}{\partial t}$ = speed of the melt front.

The description of the specific heat to ABAQUS incorporates the latent heat and the liquidus and solidus temperatures:

$$c = \begin{cases} c_0 & \text{for } T < T_s \text{ or } T > T_L \\ c_0 + \frac{L}{(T_L - T_S)} & \text{for } T_S < T < T_L \end{cases}$$

where c = specific heat described to ABAQUS

CQ = specific heat given by the specific heat correlation in Table 1

L = latent heat

TL = liquidus temperature

T§ = solidus temperature.

To compare a typical result from the two solutions, the temperature at a point located 0.5 mm into the droplet (halfway between the top of the substrate and the top of the droplet) is shown in Figure 2. Both solutions begin at the initial temperature, 2573 K, and as time elapses, the temperature falls. Due to latent heat effects, the temperature history has two points where the slope is discontinuous. The first one, at 1773 K, represents the passage of the freezing front through the location under study. The second slope discontinuity, near 0.22 seconds, occurs at the same time that the freezing front reaches the top of the droplet. The temperatures in this problem range from 303 K to 2573 K. Considering this large working temperature range, the discrepancy between the two solutions is small, and the finite difference solution and the finite element solution agree with each other.

3.2. Axisymmetric Thermal Model

While heat flows in only the axial direction in the one-dimensional model, heat diffuses in both the axial and radial directions from a single droplet that lands on a much larger substrate. To model this, a multi-dimensional model is needed. When the boundary conditions are axisymmetric or when the substrate is much larger than the droplet, the multidimensional model reduces to an axisymmetric model. Since experimental thermocouple data from Amon *et al* (1994a) will be used for future verification of the axisymmetric thermal modeling, the same geometry as that used in the thermocouple experiments is here investigated numerically. The thermocouple data comes from a specimen with a substrate thickness of 12.7 mm. The one droplet that was deposited on the substrate spreads out to cover an approximately circular area 6 mm in diameter. The solidified droplet has a height of 1.5 mm at its peak. Figure 3 shows the finite element mesh used for the axisymmetric model. The mesh simulates a 12.7 mm high substrate and a 6 mm diameter droplet. The substrate diameter was set at 10 times the droplet diameter (60 mm). In the finite element model, substantial transient heating of the substrate occurred within merely 1.5 droplet diameters around the droplet so the chosen substrate diameter is large enough that its actual diameter does not matter during the time needed to reach steady-state. Because the exact shape of the solidified droplet remains a topic for investigation, the droplet is represented in the finite element mesh by a cylinder which has approximately the same volume as the actual droplet. This results in a 0.8125 mm high simulated droplet. By setting the simulated droplet volume to match the actual droplet volume, the simulated droplet delivers the same amount of heat to the simulated substrate as the actual droplet delivers to the actual substrate. However, the substantial height difference between the simulated droplet and the actual droplet may introduce significant modeling error. In the

future, a mesh that more closely approximates the real droplet shape will be used. Nevertheless, important features of the axisymmetric model compared to the one-dimensional model will still be evident by meshing the droplet as a cylinder.

A one-dimensional model should most closely approximate the axisymmetric model at the central axis of the axisymmetric model, but the one-dimensional model is simpler to generate and converges much faster. Significant savings in computer resources are achievable if conditions can be defined under which a one-dimensional model accurately substitutes for an axisymmetric model. Figure 4 compares the temperature distribution at the central axis of the axisymmetric model to the temperature distribution of a one-dimensional model. Both models have the same droplet height, substrate height, and boundary conditions at the top and bottom. The axisymmetric model also has convection boundary conditions on the vertical walls. The solidification time (time needed for the freezing front to reach the top of the droplet) is 0.084 seconds. The temperature distribution in the one-dimensional model matches the temperature distribution along the centerline of the axisymmetric model up to the solidification time. After complete droplet solidification, the axisymmetric model cools down faster than the one-dimensional model. The difference is due to radial heat conduction absent from the one-dimensional model.

If the temperature history is needed at times greater than the solidification time, or at points near the edge of the droplet, then the axisymmetric model is more appropriate. But when studying temperature-driven events that happen much faster than complete droplet solidification, and which happen away from the edges of the droplet, a one-dimensional model can be expected to give accurate results. For example, substrate remelting, suspected to be a strong determinant of bond strength, occurs on the time scale of microseconds. This is two orders of magnitude smaller than the droplet solidification time. The predictions of the depth of substrate remelting by Amon *et al* (1994a) are thus not compromised by the one-dimensional assumption on which those predictions were based.

3.3. Convective Boundary Conditions in the Axisymmetric Thermal Model

Another thermal modeling issue is the correct boundary condition to apply to the bottom of the substrate. So far, the temperature at the bottom of the substrate has been fixed at 303 K. In Shape Deposition Manufacturing, the substrate is bolted down to a large pallet. The pallet is not a perfect 303 K heat sink, and, even with bolts clamping the substrate to the pallet, there likely remains some thermal contact resistance between the substrate and the pallet. To see the sensitivity of the temperature solution to the boundary condition at the bottom of the substrate, the models used in section 3.2 were re-run with

both the bottom of the substrate and the top of the substrate assigned the same natural convection boundary condition.

Figure 5 compares the temperature distribution at the central axis of the axisymmetric model to the temperature distribution of a one-dimensional model. As in section 3.2, the two distributions agree well before complete droplet solidification. The fixed-temperature boundary condition used in section 3.2 causes both the one-dimensional and the axisymmetric model to reach a uniform temperature of 303 K. But the convection boundary condition results in a very different uniform temperature. The one-dimensional model achieves a uniform temperature of 577 K after 14.4 seconds while the axisymmetric model achieves a uniform temperature of only 307 K after 14.8 seconds. Both models continue to convect heat to the outside, but the temperature changes due to convection are very slow compared to those due to conduction. Although radial temperature distributions are not shown, the temperature becomes uniform both axially and radially.

When studying phenomena that happen faster than complete droplet solidification, the boundary condition at the bottom of the substrate should have a minimal effect on substrate and droplet temperatures. This conclusion might not hold, however, if the substrate and the droplet have comparable thicknesses.

The axisymmetric and one-dimensional thermal problems capture two extremes for the dripping rate. The axisymmetric problem represents slow dripping, giving the substrate and the new droplet time to cool down. At the other extreme, the hypothetical case of zero time between successive droplets is equivalent to laying down one layer of molten material all at once, and this is a one-dimensional problem.

4. Mechanical Model

To study the build-up of residual stresses, a mechanical model has been formulated. This model consists of a single column of 250 second-order axisymmetric elements that represents a 3 mm layer of superheated material being deposited on a 22 mm room-temperature substrate. The elements form a uniform mesh. Appropriate boundary conditions are applied to render the problem one-dimensional. This one-dimensional mechanical model is of a single layer on a thick substrate, as was the one-dimensional thermal model. It is a reasonable initial model, corresponding to a flattened droplet on an infinite substrate. 3 mm lies within the range of typical droplet heights. The substrate can represent either one initial 22 mm substrate or an initial thinner substrate plus several layers of deposited material, all of which have been annealed. The thermal problem with the same geometry as the mechanical model has been solved using a mesh of first-order one-dimensional elements. This thermal problem has the same boundary conditions and initial

conditions as the problem from section 3.1 used to verify the thermal modeling; only the thicknesses of the droplet and the substrate have changed (see Figure 1). Figure 6 shows the temperature distribution at various times for this droplet geometry. The previously analyzed one-dimensional geometry (1 mm droplet on a 7 mm substrate) shows qualitatively the same temperature distributions as those shown in Figure 6.

To confirm the level of mesh refinement, meshes of 125 elements and 500 elements were also tested on the thermal model, the elastic model, and the elastic-plastic model. (The properties of the elastic model and the elastic-plastic model are described later). Negligible differences in the distributions of temperature and stress were found among the three meshes. The heat transfer model of section 3.1 contained 20 elements in the droplet and 140 elements in the substrate. This resolution lies between that of the coarse mesh (15 in the droplet plus 110 in the substrate) and the medium mesh (30 in the droplet plus 220 in the substrate) used in this section. The results from the meshes used in this section were independent of mesh density, suggesting that the mesh used in section 3.1 was also sufficiently refined.

While axisymmetric elements are used for the mechanical model, the one-dimensional nature of the mechanical model is maintained in two ways. First, the temperature distributions imposed onto the mechanical model do not vary along the radial coordinate ($3T/3r = 0$); the temperatures vary only with the axial coordinate ($3T/3z * 0$). Second, periodic mechanical boundary conditions are applied.

In the microcasting process, bolts hold the substrate flat against the pallet and droplets are deposited onto the substrate. The region near the center of a single deposited droplet (away from the external surface) is indistinguishable from an infinite horizontal slab. Such an infinite region can be modeled by imposing periodic boundary conditions onto a finite domain. Periodic boundary conditions require straight edges (but not necessarily vertical edges) on the finite domain to allow any number of the finite domains to fit together as they deform. Some strain in the radial direction is normally expected unless the bolts are extremely tight.

The finite domain used for all the mechanical results in this work is shown in Figure 7. A condition of zero axial displacement is applied at the bottom of the model. This corresponds to a flat substrate and also prevents rigid-body motion in the axial direction. The body is still free to expand or contract in the axial direction. The centerline undergoes zero radial displacement while the outer edge is constrained to expand (or contract) uniformly in the radial direction. Because this model maintains straight vertical edges, it allows no bending deformation.

Other one-dimensional type boundary conditions can be used, as shown in Figure 8. For instance, one can allow bending rotation of the outer edge of the model while demanding that the outer edge deforms as a line. This would correspond to deposition onto an unbolted substrate. Or one can demand both zero bending and zero radial expansion, which corresponds to a very secure bolting condition. Regardless, the outer edge must deform as a straight line to maintain the periodic boundary conditions and therefore the one-dimensional nature of the problem.

4.1. Elastic Behavior

In this section, a mechanical model is presented which assumes linear elastic behavior in the droplet and substrate. Results from an elastic solution are easy to interpret. Effects of plastic yielding and creep will be added later. As an additional benefit, the purely elastic material model has a steady-state stress solution obtainable from calculations that can be easily done by hand. Thus, this model will detect incorrect use of ABAQUS to solve the mechanical portion of the problem. For instance, if the finite element stress result disagrees with the hand calculations, then perhaps the boundary conditions are not being described correctly to ABAQUS, or the temperature history at a particular node in the thermal model is being imposed onto a node in the mechanical model that has a different position.

The development of stresses in this problem is shown in Figure 9, which plots normalized radial stress as a function of depth. Although changing the mechanical properties has no effect on the normalized stress, the mechanical properties used are typical of carbon steel: Young's modulus E = 200 GPa, Poisson's ratio v = 0.27, and linear thermal expansion coefficient **a** = 12 x 10^/K. In the model, these mechanical properties are set to be independent of temperature, and the use of a constant linear thermal expansion coefficient neglects phase changes. The initial temperature of the droplet is 2573 K and its final temperature is 303 K, for a AT of 2270 K. The droplet extends over a depth of zero to 3 mm while the substrate extends from 3 mm down to 25 mm. Initially, there is no stress, but as the hot droplet cools, tensile stresses build up in the droplet. At the same time, the top of the substrate heats up and compressive stresses build up at the top of the substrate. As steady-state is approached, the top of the substrate cools and the magnitude of the compression drops. Throughout the process, the mechanical boundary conditions allow a net moment but zero net radial force (i.e., Jan-dz = 0). The requirement of zero net radial force induces compression in the substrate in order to balance the tension in the newly dripped layer.

By imposing equal uniform radial strains in the droplet layer and substrate, a force balance predicts the final stresses to be

$$\frac{a_d (1 - \nu)}{E \alpha \Delta T} = \frac{1}{\left(\frac{d}{s}\right)} \quad \text{and} \quad \frac{\sigma_s (1 - \nu)}{E \alpha \Delta T} = \frac{-1}{\left(\frac{d}{s}\right)}$$

where a_d = final radial stress in the droplet

a_s = final radial stress in the substrate

d = thickness of the droplet = 0.003 m

s = thickness of the substrate = 0.022 m

The final normalized residual stress values are predicted to be 0.88 in the droplet and -0.12 in the substrate, which agrees with the finite element result.

4.2. Elastic-Plastic Behavior

In this section, the effects of plasticity are studied by assigning a temperature-independent yield stress of 300 MPa to the carbon steel model used in section 4.1. 300 MPa corresponds to a typical yield stress for medium carbon steel. In order to learn what features are due to the existence of a yield stress, a simple form should be chosen for the yield stress, and the simplest form is a constant yield stress. Using the previous purely elastic model, both the droplet and the substrate are capable of sustaining *any* stress, even when the droplet temperature is higher than the solidus temperature. In this plastic model, the material yields at 300 MPa when its temperature is below the solidus temperature. Above the solidus temperature, the yield stress is set to 1% of the solid value, to 3 MPa. Because the numerical solver for a solid material model requires a non-zero yield stress, the liquid is treated as a material with a "yield stress" that is small compared to the yield stress of the solid. This approximation should not hinder accuracy or interpretation of the results because a stress of 3 MPa is small even compared to typical elastic stresses that build up at early times in the substrate.

Figures 10a and 10b show how the stresses develop in an elastic-plastic material. The yield stress of 300 MPa is apparent because all the curves flatten out when they reach a magnitude of 300 MPa and they are contained inside ±300 MPa. An important feature not seen in the purely elastic material is the cycling in the top of the substrate (just beneath the droplet). First, the top of the substrate heats up and tends to expand, and compressive stress builds up. The compressive stress becomes so large that the top of the substrate yields in compression. The substrate then cools off, contracts, and yields in tension. At steady state, high stresses are present in the entire droplet and the top portion of the substrate. The entire droplet and the top portion of the substrate are yielded in tension. To

satisfy the boundary condition of zero net radial force, the bottom of the substrate is yielded in compression.

4.3. Elastic-Plastic Behavior with Creep

To account for the effect of creep, a secondary (steady-state) creep law for a medium carbon steel in the austenitic phase is chosen (Thomas *et al.*[9] 1987). The other mechanical properties (yield stress, elastic moduli, and linear expansion coefficient) remain the same as in section 4.2. This creep law assumes no phase changes.

$$\dot{\varepsilon} = A\,(\sinh(B\bar{\sigma}))^n \exp\left(-\frac{C}{T}\right)$$

where $\dot{\varepsilon}$ = creep strain rate in reciprocal seconds

$\bar{\sigma}$ = Mises equivalent stress in MPa (not Pascals)

T = temperature in Kelvin

A = $9O7xlO^{10}$

B = 0.0356

C = 41938

n = 6.9

This creep law is a secondary creep law applicable under the conditions of constant stress and steady state. Because the temperatures, and therefore the stresses, in the droplet and substrate continually change, a primary creep law should be used for greater accuracy. Such a creep law will be used in future work, coupled with temperature-dependent material properties.

The one-dimensional mechanical model with a steady-state creep law results in the stresses shown in Figures 11a and 11b. At high temperatures, creep strains do not permit regions of high stress to persist. This is evident by comparing Figure 10a to Figure 11a at early times in the top of the substrate. In the elastic-plastic case, stresses below the yield point build up, but when creep is allowed, stresses that build up cause flow, which relaxes the stresses.

The exponential factor in the creep law imposes a very steep drop in the creep rate as the temperature is decreased. Thus, at later times (after the absolute temperature drops to less than about half of the solidus temperature), creep becomes negligible, and the model including creep behaves very much like the elastic-plastic model. Both the creep model and the elastic-plastic model show a cycle of compression followed by tension in the top of the substrate. In the steady-state, stress distributions in both models are similar (compare Figures 10b and 11b). There is a difference in the elastic zone located near the middle of both models, but the general trend is the same in both: There is a tensile zone which

encompasses both the droplet and the top of the substrate, then an elastic transition zone, followed by a yielded compressive zone at the bottom of the substrate. Therefore, although creep alters stresses at *early* times, it has a minimal effect on final stress distributions.

In both elastic-plastic models (with and without creep), a portion of the substrate is compressed at early times but ends up in tension at steady-state. That portion extends from a depth of 3 mm down to about 12 mm; it spans 3 droplet heights. The high stresses seen in Figures 10b and 1 lb are likely to occur during part manufacture. It is likely that these stresses will be substantially relaxed once the part is completed and removed from the pallet upon which it is built.

5. Conclusions

In this study thermo-mechanical models have been presented for a single droplet or layer of carbon steel deposited onto a thick carbon steel substrate, simulating the effects of droplets of a manufactured part being deposited onto a thick pallet In thermal modeling, a simple one-dimensional model gives temperatures that are very close to an axisymmetric model, provided that: i) the comparison is made for times before the droplet completely solidifies, and ii) the region of interest is close to the center axis of the droplet. Under these conditions, the boundary condition at the bottom of the substrate also makes little difference.

Residual stresses near the yield point are likely during the manufacture of carbon steel parts. In particular, the newly deposited layer will reach the yield stress in tension. It is likely that these stresses will be substantially relaxed, however, once the part is completed and removed from the pallet. Creep plays an important role at high temperatures in the qualitative development of the stress distribution, but the droplet and substrate stay at high temperatures only for short times for the case of the first droplet. Due to the short duration of exposure to high temperatures, the final stress distribution predicted from the elastic-plastic model is similar to the final stress distribution predicted from adding creep to the elastic-plastic model.

Future work in this area will include more axisymmetric modeling of the thermal problem in order to obtain results for comparison with experimental thermocouple data from Amon *et al.* (1994a). Future work will also include one-dimensional modeling of the mechanical problem to account for temperature-dependent mechanical properties (Young's modulus, coefficient of thermal expansion, yield stress, primary [transient] creep) and axisymmetric modeling to better understand the mechanical constraints imposed on deposited droplets. To make the models more realistic, the axisymmetric models will assume the droplet to take on the shape of a portion of a sphere instead of a cylinder.

6. Acknowledgements

The authors gratefully acknowledge financial support by the Office of Naval Research under Grant No. NOOO14-94-1-0183. This work is also supported by the Engineering Design Research Center, an Engineering Research Center of the National Science Foundation, under Grant No. EEC-8943164.

7. References

Amon, C.H., Merz, R., Prinz, F.B., and Schmaltz, K.S., 1994a, "Thermal Modeling and Experimental Testing of MD* Spray Shape Deposition Processes," Proceedings of the Tenth International Heat Transfer Conference, Brighton, U.K., pp.321-326.

Amon, C.H., Schmaltz, K.S., Merz, R., and Prinz, F.B., 1994b, "Numerical Modeling and Experimental Testing of Metal Droplet Deposition Heat Transfer with Substrate Remelting as Applied to the Microcasting Deposition Process," Engineering Design Research Center report 24-116-94, Carnegie Mellon University, Pittsburgh, Pennsylvania.

El-Kaddah, N., McKelliget, J., and Szekely, J., 1984, "Heat Transfer and Fluid Flow in Plasma Spraying," Metallurgical Transactions B, Vol. 15B, pp. 59-70.

Gao, F. and Sonin, A.A., 1993, "The Physics of Digital Microfabrication with Molten Microdroplets," Proceedings, Solid Freeform Fabrication Symposium, Austin, Texas, August 1993, pp. 237-244.

Landau, H.G., Weiner, J.H., and Zwicky, E.E. Jr., 1960, "Thermal Stress in a Viscoelastic-Plastic Plate with Temperature-Dependent Yield Stress," Journal of Applied Mechanics, Vol. 27, Transactions of the ASME, Vol. 82, pp. 297-302.

Merz, R., 1994, "Shape Deposition Manufacturing," Dissertation, Electrical Engineering Department, Technical University of Vienna.

Merz, R., Prinz, F.B., Ramaswami, K., Terk, M., and Weiss, L.E., 1994, "Shape Deposition Manufacturing," Proceedings, Solid Freeform Fabrication Symposium, Austin, Texas, August 1994.

Schmaltz, K.S., 1994, Thesis Proposal, Mechanical Engineering Department, Carnegie Mellon University, Pittsburgh, Pennsylvania.

Thomas, B.G., Samarasekera, I.V., and Brimacombe, J.K., 1987, "Mathematical Modeling of the Thermal Processing of Steel Ingots: Partll. Stress Model," Metallurgical Transactions B, Vol. 18B, pp. 131-147.

Trapaga, G., and Szekely, J., 1991, "Mathematical Modeling of the Isothermal Impingement of Liquid Droplets in Spraying Processes," Metallurgical Transactions B, Vol. 22B, pp. 901-914.

Weiner, J.H., and Boley, B.A., 1963, "Elasto-Plastic Thermal Stresses in a Solidifying Body," Journal of the Mechanics and Physics of Solids, Vol. 11, pp. 145-154.

Zabaras, N., Ruan, Y., and Richmond, O., 1991, "On the Calculation of Deformations and Stresses During Axially Symmetric Solidification," ASME Journal of Applied Mechanics, Vol. 58, pp. 865-871.

Table 1. Temperature-Dependent Thermal Properties

Correlations used from 298 K to 3273 K:

T = temperature in Kelvins

Density in $\frac{kg}{m^3}$

$$\left(7.9 - \frac{T - 273}{1500}\right) \times 1000$$

Specific Heat in $\frac{J}{kg\text{-}K}$

$$\left(0.06 + 0.000036 \times (T - 273) + 0.12 \times \exp\left(\frac{-600}{T - 273}\right)\right) \times 4184$$

Diffiisivity in $\frac{}{s}$

$$\left(0.2 + 0.00003 \times (T - 273) - 0.225 \times \exp\left[\frac{-30}{T - 273}\right]\right) \times 1000$$

In this work, conductivity was defined as diffiisivity x density x specific heat. However, a correlation that gives nearly the same result is:

Conductivity in $\frac{W}{m\text{-}K}$

$$(0.1016 - 5.065 \times 10^{-5} \times (T - 273) + 2.2 \times 10^{-11} \times (T - 273)^2) \times 418.4$$

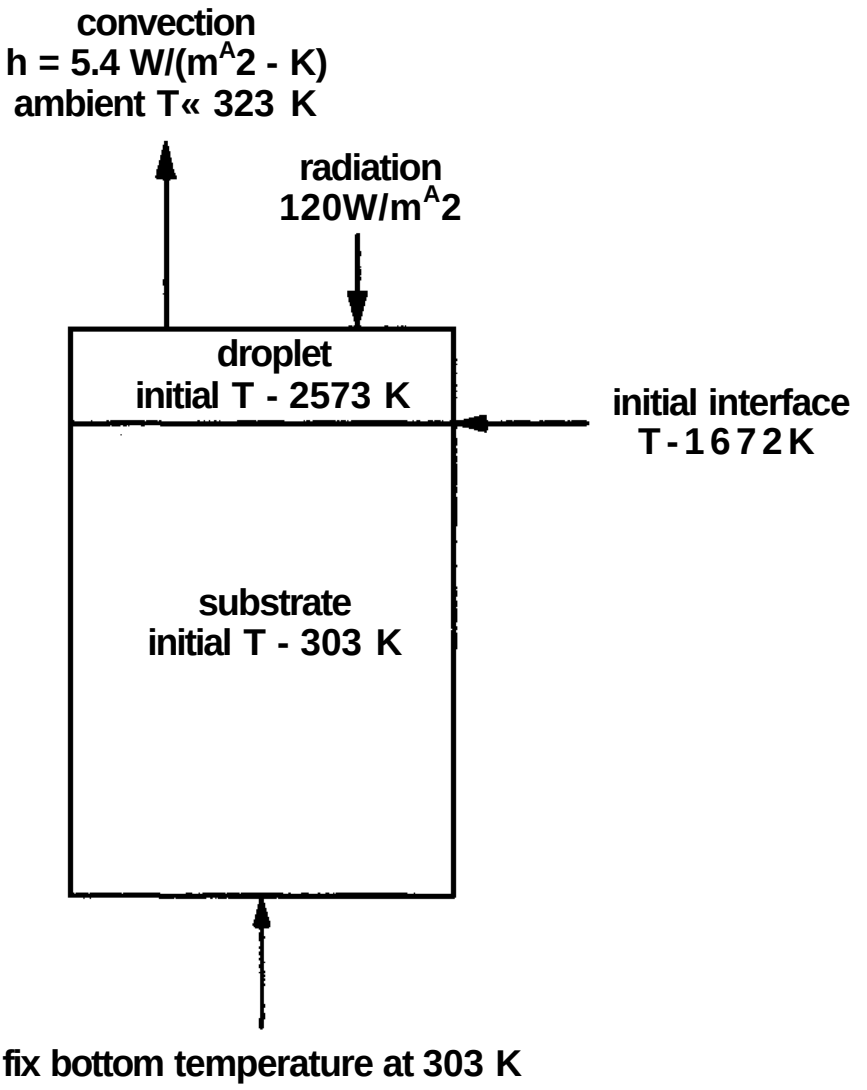

Figure 1. Boundary conditions and initial conditions of one-dimensional thermal problem.

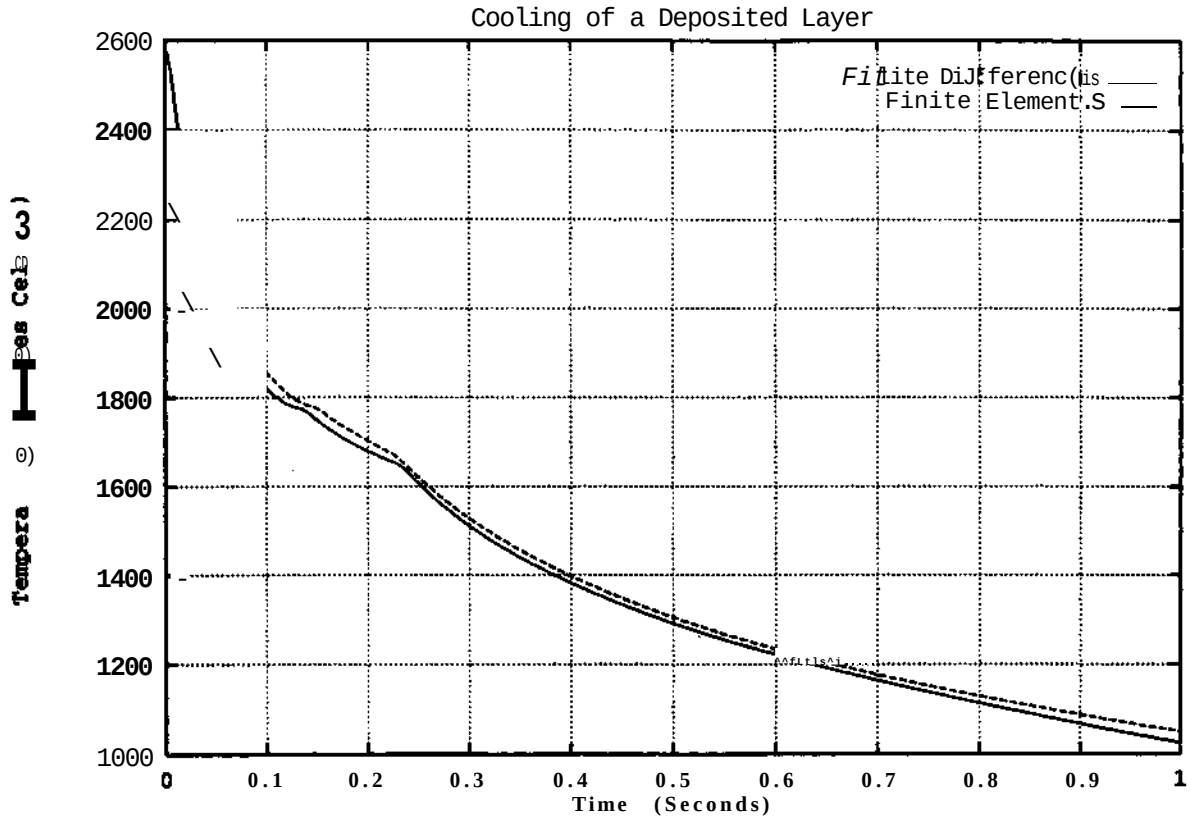

Figure 2. Temperature history halfway through the droplet.

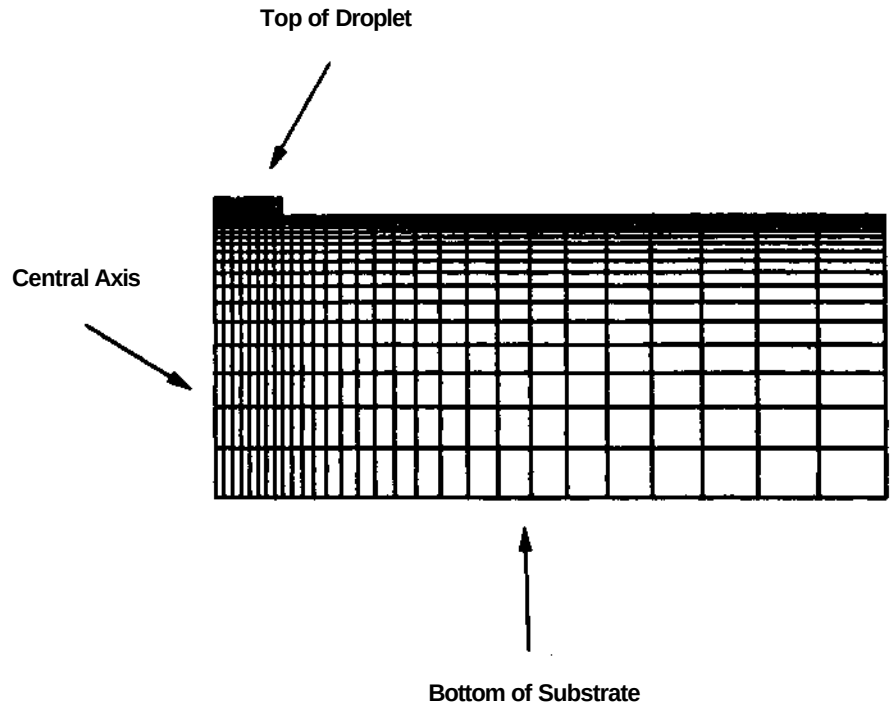

Figure 3. Mesh for axisymmetric model.

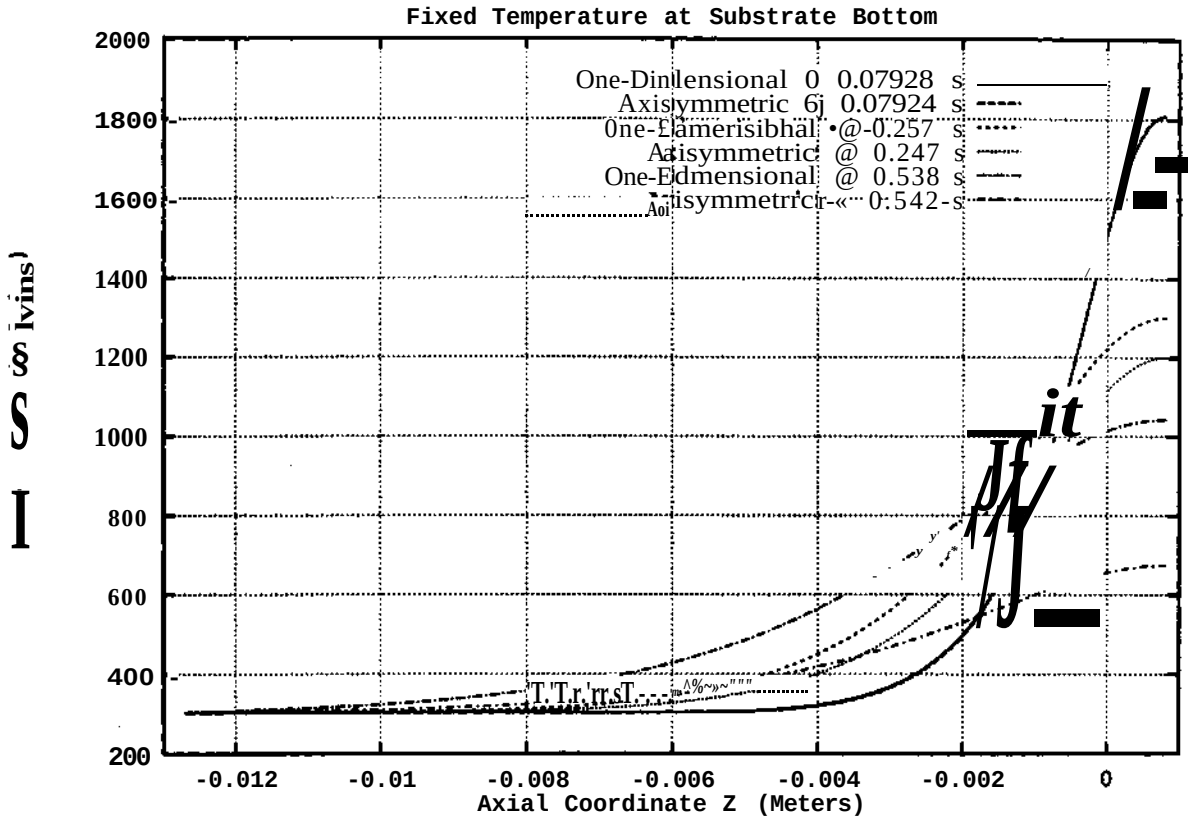

Figure 4. Temperature distributions along the axis of the axisymmetric model and the one-dimensional model with a fixed temperature boundary condition beneath the substrate.

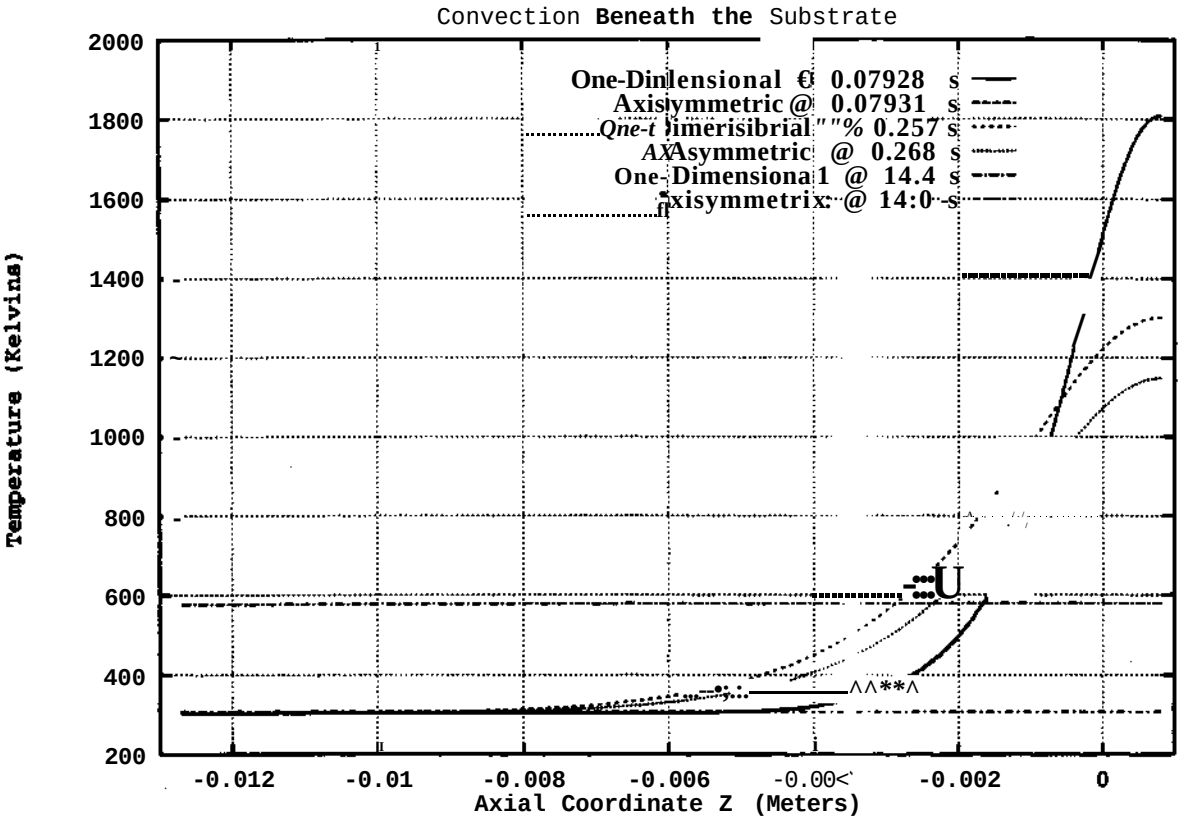

Figure 5. Temperature distributions along the axis of the axisymmetric model and the one-dimensional model with a convection boundary condition beneath the substrate.

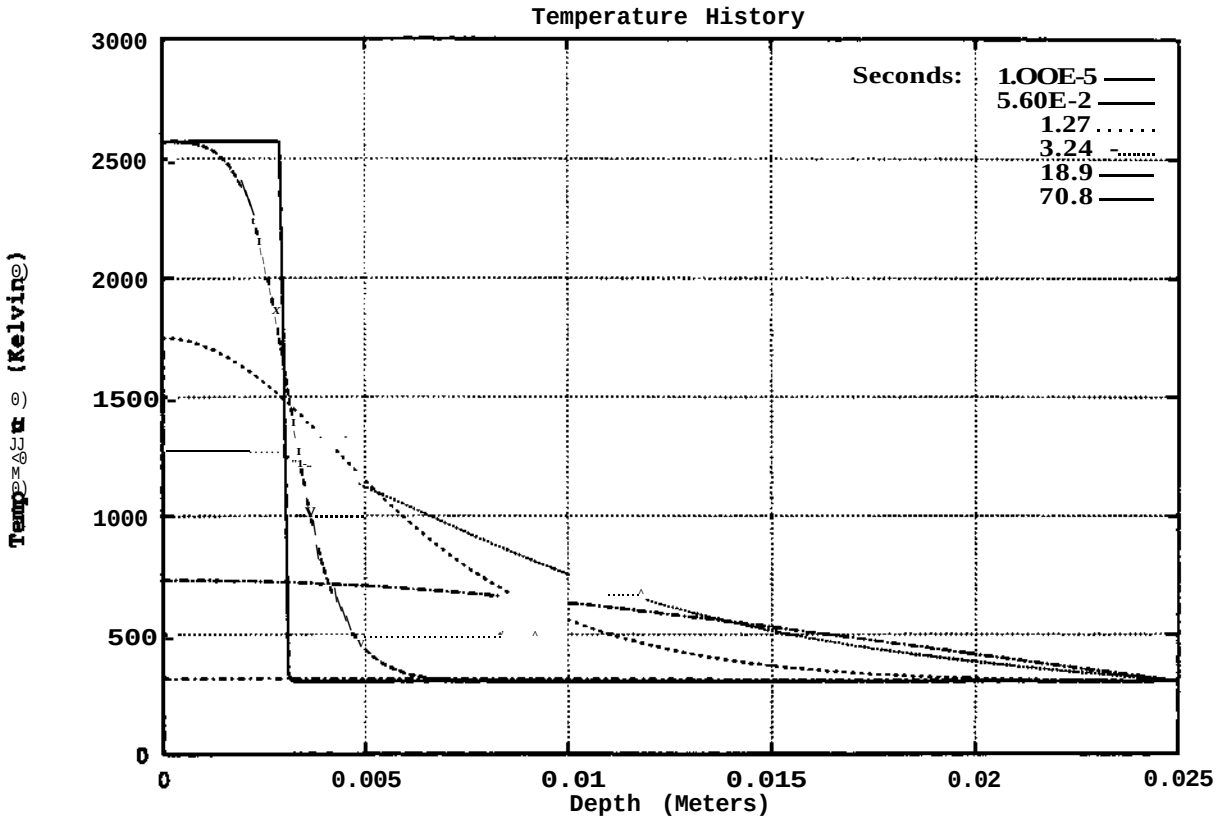

Figure 6. Temperature distributions for the 3 mm droplet / 22 mm substrate one-**dimensional model.**

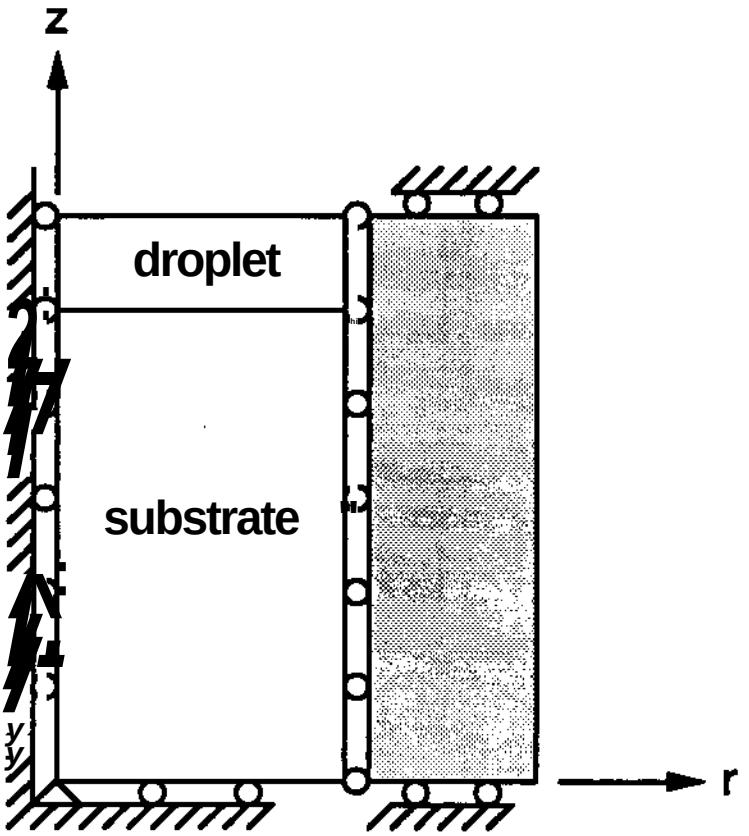

Figure 7. Mechanical boundary conditions used.

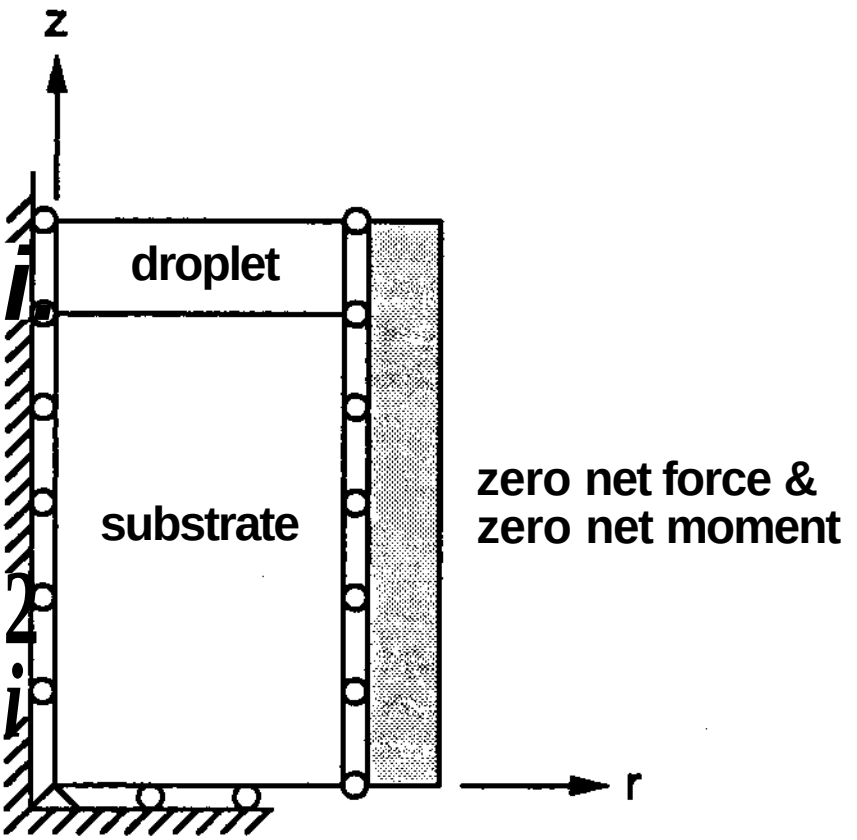

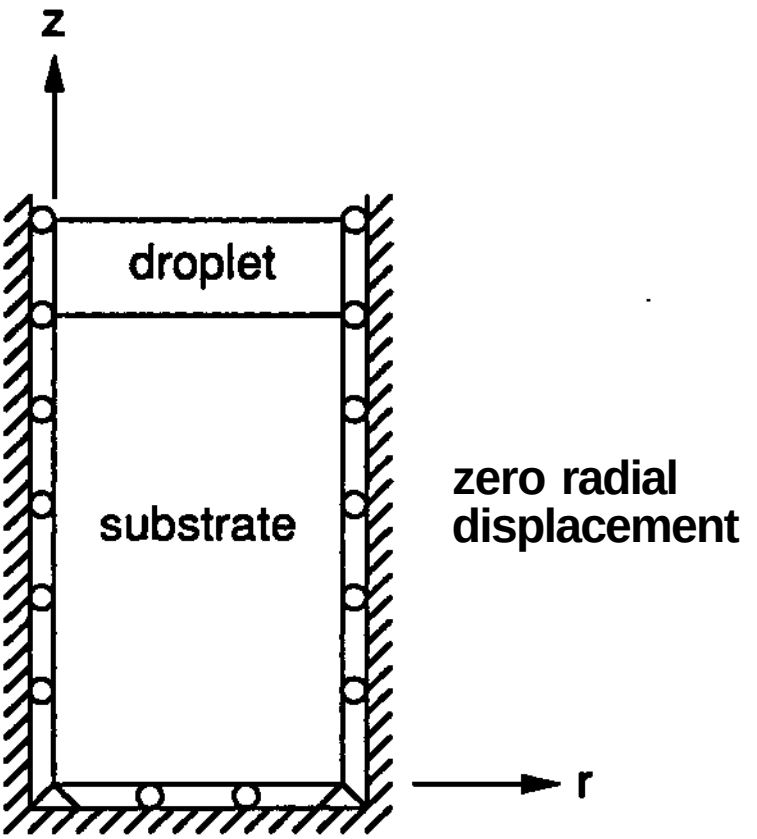

Figure 8. Alternate mechanical boundary conditions.

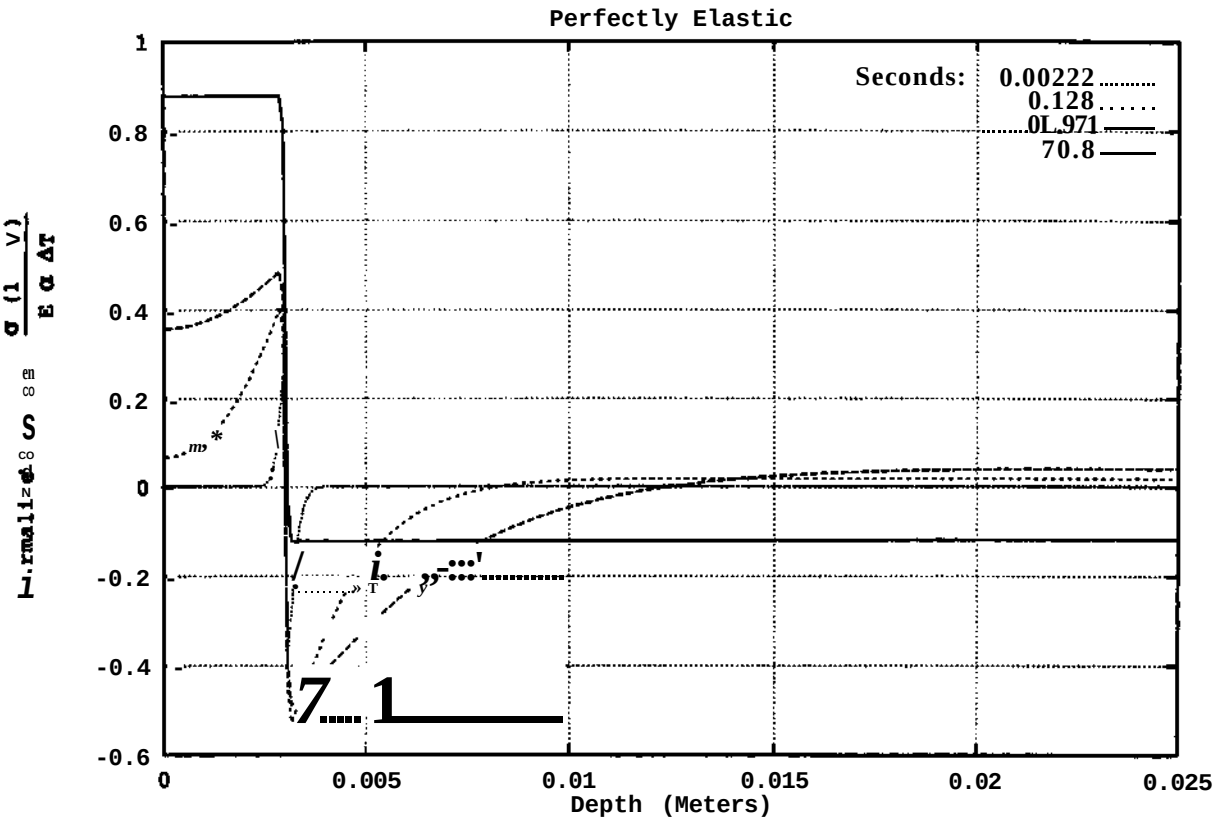

Figure 9. Stress distributions for the elastic model.

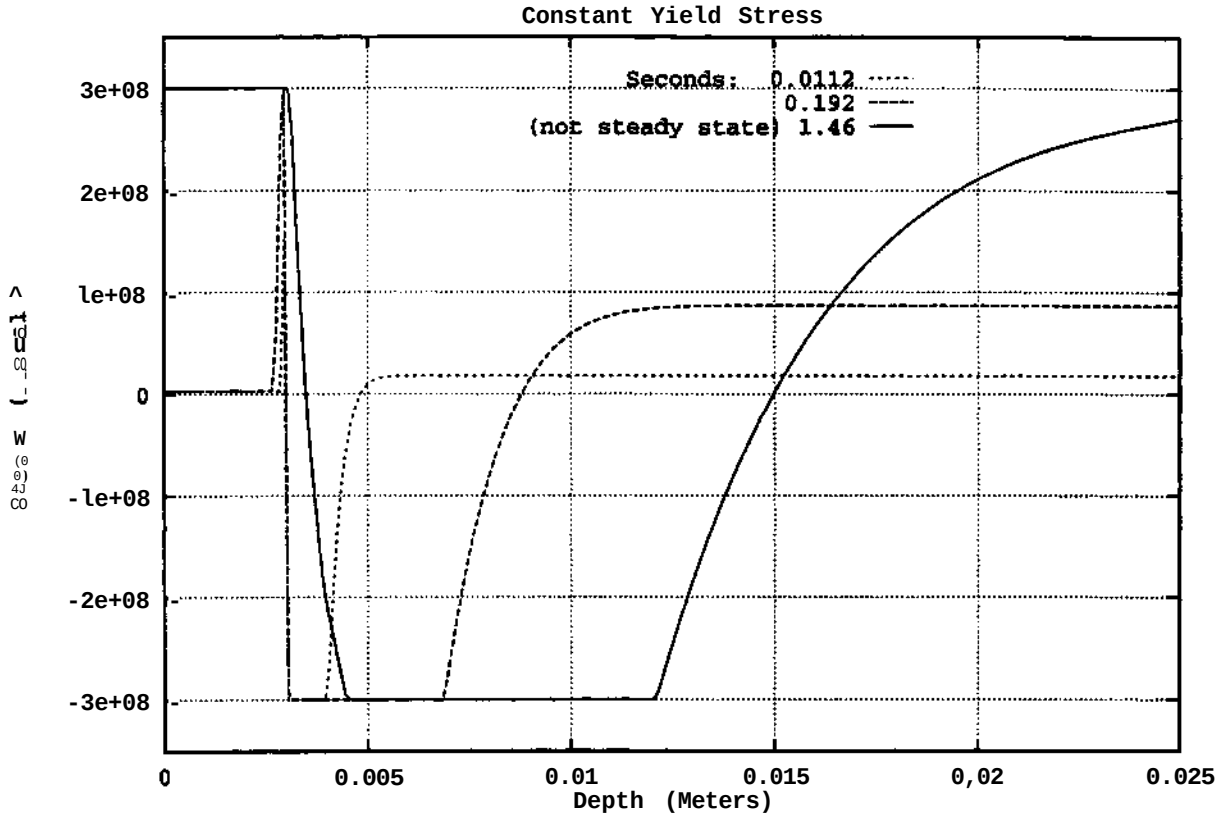

Figure 10a. Stress distributions for the elastic-plastic model at early times.

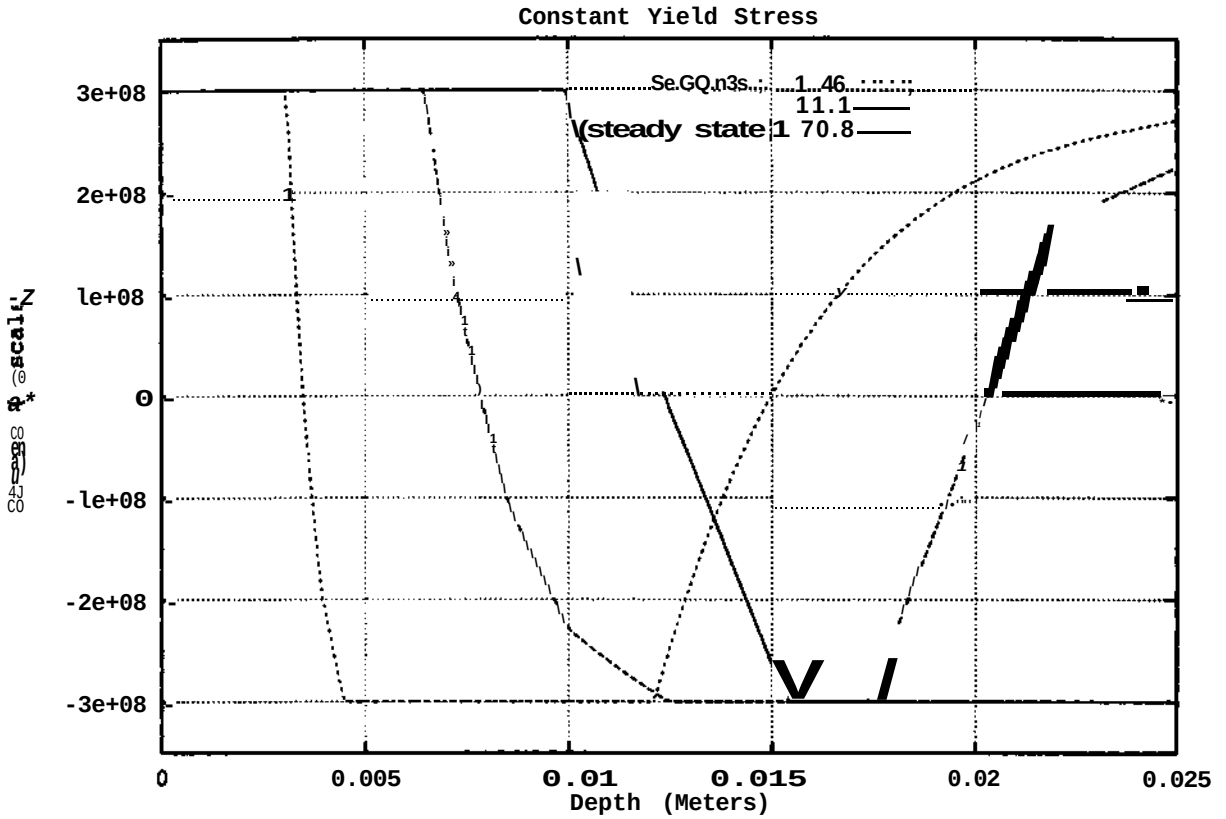

Figure 10b. Stress distributions for the elastic-plastic model at later times.

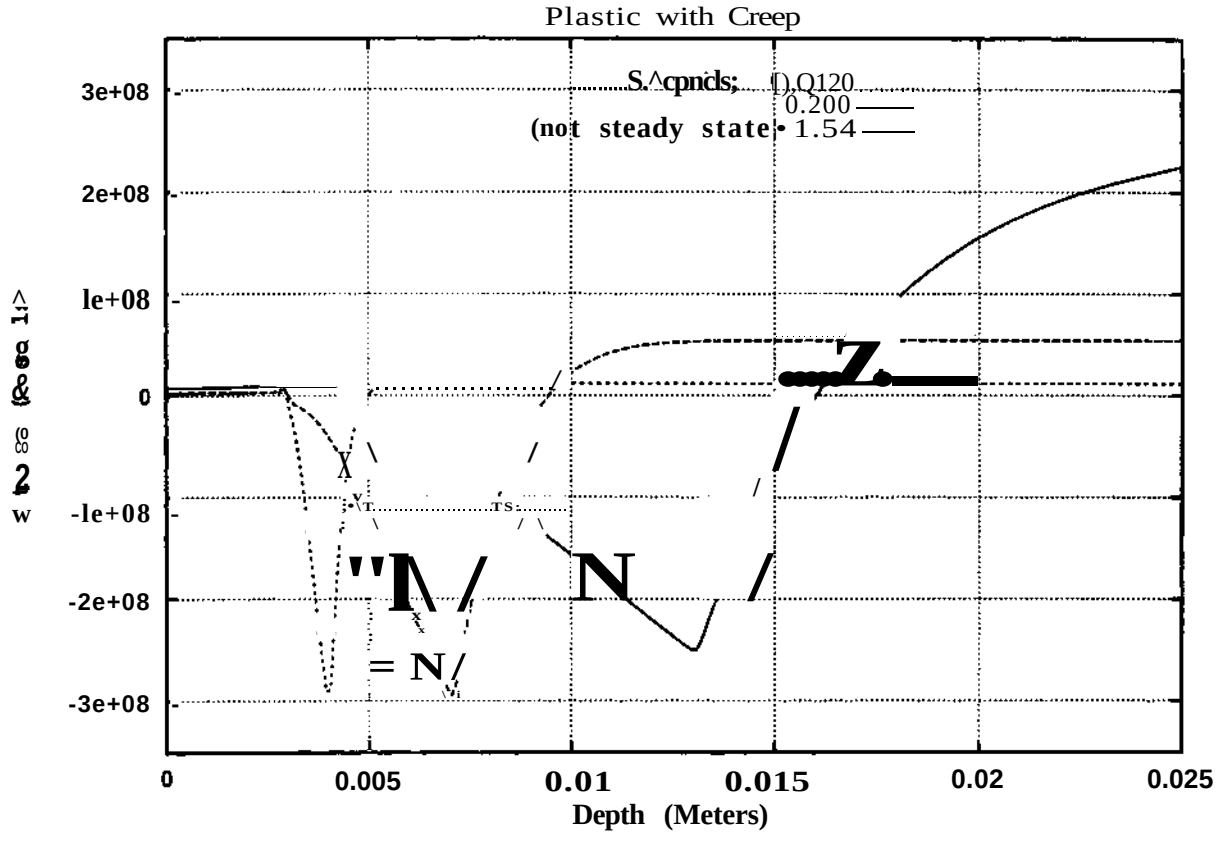

Figure 1 la. Stress distributions for the creep model at early times.

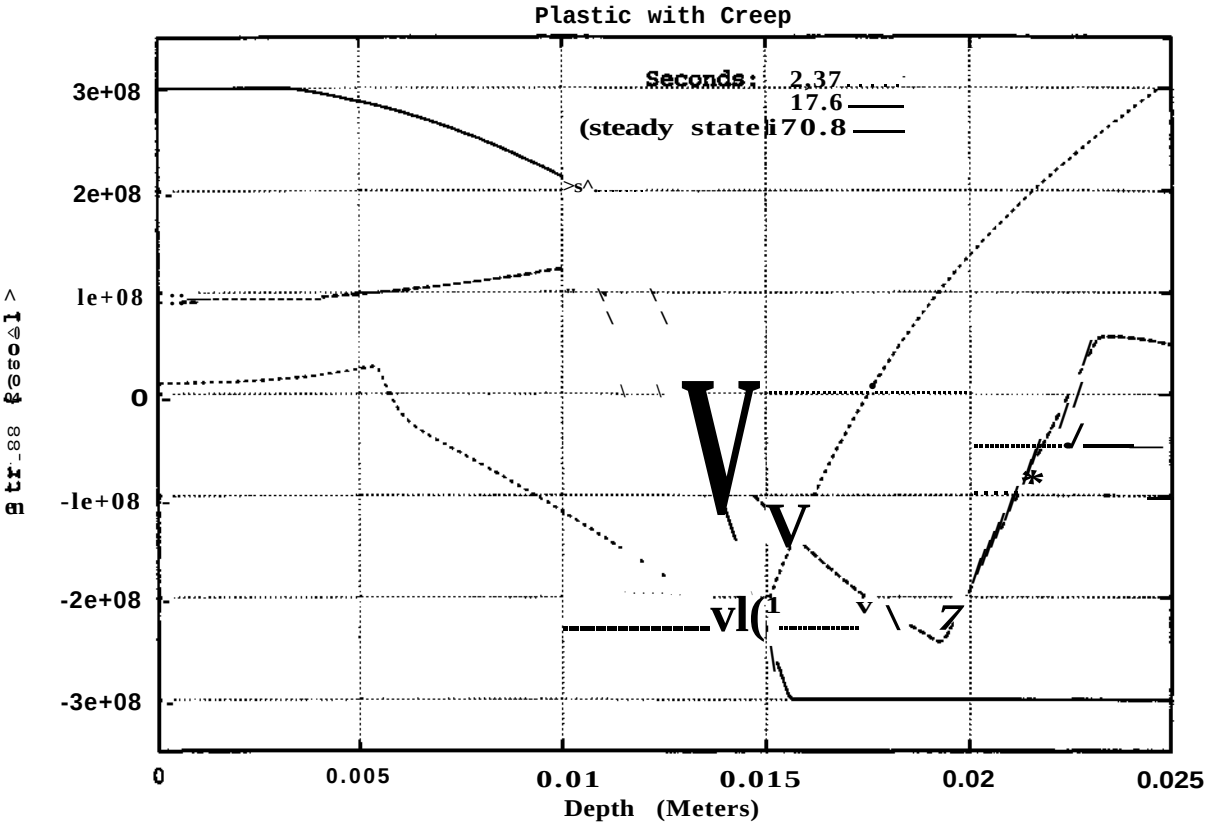

Figure lib. Stress distributions for the creep model at later times.